Gang Xu
Philip S. Kemp
Joyce A. Hwu
Adam M. Beagley

Department of Biomedical Engineering,
Washington University,
Saint Louis, MO 63130

Philip V. Bayly
Department of Mechanical, Aerospace, and Structural Engineering and Department of Biomedical Engineering,
Washington University,
Saint Louis, MO 63130

Larry A. Taber[1]
Department of Biomedical Engineering and Department of Mechanical, Aerospace, and Structural Engineering,
Washington University,
Saint Louis, MO 63130
e-mail: lat@wustl.edu

Opening Angles and Material Properties of the Early Embryonic Chick Brain

Mechanical forces play an important role during brain development. In the early embryo, the anterior end of the neural tube enlarges and differentiates into the major brain subdivisions, including three expanding vesicles (forebrain, midbrain, and hindbrain) separated by two constrictions. Once the anterior neuropore and the spinal neurocoel occlude, the brain tube undergoes further regional growth and expansion in response to increasing cerebrospinal fluid pressure. Although this is known to be a response to mechanical loads, the mechanical properties of the developing brain remain largely unknown. In this work, we measured regional opening angles (due to residual stress) and stiffness of the embryonic chick brain during Hamburger–Hamilton stages 11–13 (approximately 42–51 h incubation). Opening angles resulting from a radial cut on transverse brain slices were about 40–110 deg (depending on region and stage) and served as an indicator of circumferential residual stress. In addition, using a custom-made microindentation device and finite-element models, we determined regional indentation stiffness and material properties. The results indicate that the modulus is relatively independent of position and stage of development with the average shear modulus being about 220 Pa for stages 11–13 chick brains. Information on the regional material properties of the early embryonic brain will help illuminate the process of early brain morphogenesis.
[DOI: 10.1115/1.4000169]

Keywords: biomechanics, morphogenesis, microindentation, residual stress, neuroepithelium

1 Introduction

The early development of the embryonic chick brain closely resembles that of the embryonic human brain [1–4]. In both cases the brain expands and differentiates at the anterior end of the neural tube into several major subdivisions, including three bulging vesicles or "hills" (prosencephalon or forebrain, mesencephalon or midbrain, and rhombencephalon or hindbrain) (Fig. 1(*d*)). The hills are separated by the forebrain-midbrain (FM) and midbrain-hindbrain (MH) constrictions or "valleys" (Fig. 1(*d*)). Once the brain cavity is sealed by occlusion of the anterior neuropore and the spinal neurocoel (by Hamburger–Hamilton [5] stage 12 for the chick brain), the brain tube undergoes further regional growth and expansion (Fig. 1). Proper vesicle expansion is a crucial step in normal brain development, as anomalies in this process are linked to severe neurological disorders, including hydrocephalus (abnormal vesicle enlargement caused by excessive accumulation of cerebrospinal fluid) and anencephaly (absence of most of the brain caused by a defect in neural tube closure).

While the morphological changes that occur during early brain development are well known, the mechanisms of vesicle formation and enlargement remain unclear. After the chick brain cavity is sealed (by stage 12), a cerebrospinal fluid pressure of about 2–3 mm H_2O has been measured and it increases gradually as brain development proceeds [6,7]. During the same period, rapid cavity expansion and tissue growth occur [3]. It has been shown that the luminal pressure is necessary for early brain enlargement as removal of normal pressure by intubation results in reduced growth and cavity size [1]. The dependence of early brain growth on pressure is further demonstrated by immediate brain expansion that follows precocious occlusion of the spinal neurocoel before stage 11 [8]. Therefore, mechanical forces play an important role in early brain development.

The early brain tube is composed of a single layer of neural stem cells called the neuroepithelium [9]. The nuclei of these cells migrate radially within the cell body during the cell cycle forming a pseudostratified structure [9]. The nuclei are located near the outside surface of the brain tube where DNA synthesis occurs. They move toward the lumen as the cell cycle proceeds and are close to the luminal side of the brain when mitosis occurs. During morphogenesis compressive stresses slow, whereas tensile stresses increase, cell proliferation (see the review by Wozniak and Chen [10]). It has also been shown that sustained pressure promotes higher neuroepithelial proliferation [3,6]. Therefore, rapid proliferation of the neuroepithelium could result from tensile stresses in the early brain caused by increasing pressure. However, the stress distribution in the embryonic brain has not yet been determined. Mean wall stresses can be estimated using Laplace's law but detailed transmural distributions must be computed using a more complex model, which requires information on residual stresses (stresses in the tissue when all external loads are removed) and material properties. Such data for the early brain tube are not yet available.

In this work, we measured regional opening angles (residual stress) and stiffness of the embryonic chick brain during Hamburger–Hamilton stages 11–13 (approximately 42–51 h incubation). Opening angles of 40–110 deg (depending on region and stage) were measured following transmural cuts in thin brain slices. In addition, using a custom-made microindentation device, we probed the regional stiffness of the brain tube and finite-element models provided estimates for the modulus of the brain at different stages. The information on the regional material properties should help illuminate mechanical processes in early brain morphogenesis.

[1]Corresponding author.
Contributed by the Bioengineering Division of ASME for publication in the JOURNAL OF BIOMECHANICAL ENGINEERING. Manuscript received May 18, 2009; final manuscript received July 24, 2009; accepted manuscript posted September 4, 2009; published online December 9, 2009. Assoc. Editor: Michael Sacks.

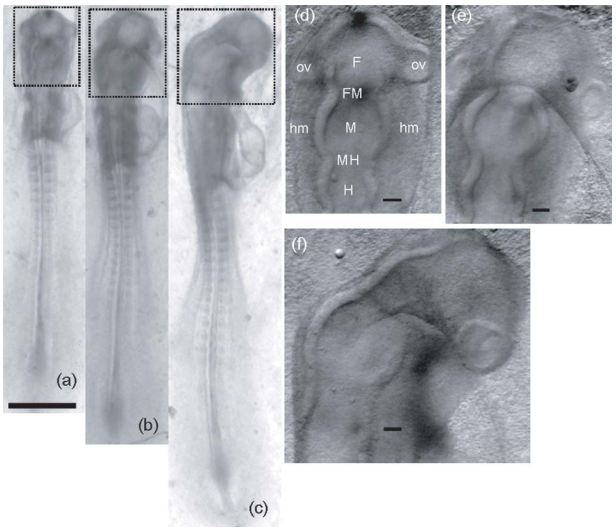

Fig. 1 Early embryonic chick brain. (*a*)–(*c*) Dorsal view of the chick embryo at stages 11, 12, and 13, respectively. Embryos in (*a*)–(*c*) have the same scale bar, which is 1 mm. (*d*)–(*f*) Close-ups of the brain region from the embryo in (*a*)–(*c*) (dashed rectangle), respectively. Major subdivisions of the brain include three vesicles: forebrain (*F*), midbrain (*M*), and hindbrain (*H*) with two constrictions, which are FM valley and MH valley. The optic vesicles (ov) are also shown. The brain is surrounded by head mesenchyme (hm) (scale bar is 100 μm).

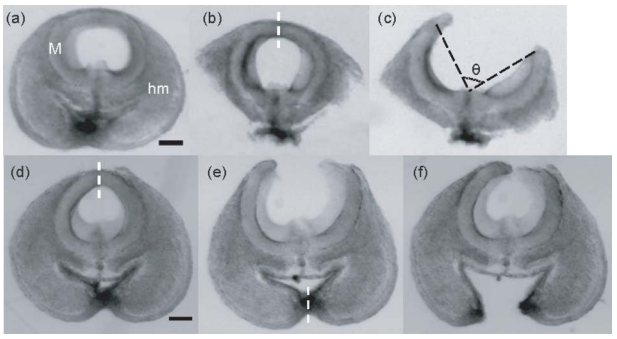

Fig. 2 Microdissection of the early embryonic chick brain. (*a*) A thin midbrain slice (*M*) from a stage-12 chick embryo surrounded by head mesenchyme (hm), (*b*) the brain slice after most surrounding tissue was removed, and (*c*) a radial cut on the dorsal side of the brain slice (indicated by dashed line in (*b*)). The resulting approximate zero-stress state of the brain slice is characterized by the opening angle (θ). (*d*)–(*f*) Demonstration of how surrounding tissue affects the opening angle of a stage-12 midbrain slice. Dashed lines in (*d*) and (*e*) are radial cuts on the slice that resulted in the shapes shown in (*e*) and (*f*), respectively (see text for details). All images are at the same scale with scale bars representing 100 μm.

2 Materials and Methods

Fertile White Leghorn chicken eggs (Sunrise Farms, Catskill, NY) were incubated at 38 °C for 42–52 h to yield embryos at stages 11, 12, and 13 (Figs. 1(*a*)–1(*c*)) of Hamburger and Hamilton [5]. Embryos were extracted from the eggs using Whatman filter paper rings [11] and washed in phosphate-buffered saline (PBS) solution at room temperature. The differentiated brain regions along each embryonic neural tube can easily be identified under the microscope (Figs. 1(*d*)–1(*f*)).

2.1 Microdissection. Thin slices (approximately 100 μm in thickness) were obtained by cutting the brain tube transversely with a pair of fine spring scissors (Fine Science Tools, Foster City, CA) (Fig. 2(*a*)). Dissections revealed that surrounding head mesenchyme can affect the opening angles of the brain slices (Figs. 2(*d*)–2(*f*)). Hence, most of these tissues were removed from the brain slice using sharp glass micropipettes (Fig. 2(*b*)). The scissors were then used to make a radial (transmural) cut on the dorsal side of the brain slice (Fig. 2(*c*)) to release circumferential residual stress. The resulting approximate zero-stress state of the brain slice was characterized by the opening angle (θ) between two radii joining the midpoint to the two tips of the inner wall (see Fig. 2(*c*)). The opening angle was measured from an image acquired about 15 min after the radial cut. All the microdissection experiments were conducted in PBS at room temperature. Due to complications from the optic vesicles, sections from the forebrain region are not included.

All the samples in Figs. 1 and 2 were imaged with a video camera (COHU, Model 4915, San Diego, CA) mounted on a dissecting microscope (Leica Microsystems, Model MZ8, Bannockburn, IL). Images were acquired by a frame grabber (FlashBus MV, Integral Technologies, Indianapolis, IN) and imaging software (SigmaScan Pro V.5.0, Systat Software, San Jose, CA).

At each stage, seven to ten slices were obtained for each region, except the MH valley region at stage 13 (four slices). To compare opening angles between regions at a certain stage or between stages at a certain region, one-way ANOVA tests were used followed by Tukey's all-pair comparison. For all statistical analyses, 0.05 was chosen as the significance level.

2.2 Microindentation Tests. Regional stiffness of the brain tube at each developmental stage was probed by a custom-made microindentation device, which was previously designed for testing the embryonic chicken heart [12]. Briefly, one end of a glass cantilever beam (about 66 μm in diameter) is attached to a piezoelectric stage (PZS-200, Burleigh Instruments, Fishers, NY) through a rigid glass pipette. The other (free) end is joined perpendicularly to a short glass cylindrical indenter tip (with a flat face about 20 μm in diameter). A manually marked ink spot on the indenter tip was used to track its displacement (Fig. 3(*a*)). The beam stiffness was measured to be about 1 mdyn/μm (10 nN/μm).

After removing most of the surrounding tissues, the brain tube was isolated from the embryo by removing the part of the neural tube below the hindbrain region. Hence, all tests were conducted on brains with no internal pressure. The ventral side of the brain at a given region was held by suction on a glass pipette (about 100 μm in diameter) and positioned under the microscope with a micromanipulator. The indenter tip was positioned directly opposite the glass pipette to indent the dorsal side of the brain, perpendicular to the brain surface (Fig. 3(*a*)). The piezoelectric stage was controlled by an amplified 0.1 Hz sawtoothlike voltage signal. The beam and the indenter tip were then driven to approach or retract away from the brain tube at a speed of approximately 46 μm/s. The initial distance of the brain tube and the indenter tip was controlled such that the indenter tip either would not touch the brain tube when approaching (control) or would gently indent the brain tube at the specified region (Fig. 3(*b*)). All microindentation experiments were conducted at room temperature with the sample brain, the cantilever beam, and the indenter tip submerged in PBS. The dorsal side of the brain is ideal for indentation because there is little mesenchymal tissue on this side.

The displacements of the indenter tip during control and indentation were obtained from video micrographs by tracking the ink spot on the indenter tip, from which the beam deflection and tissue indentation depth were determined (Fig. 3(*c*)). The product of beam deflection and beam stiffness yields the indentation force (see Fig. 3(*c*) and Ref. [12] for more details). Finally, the slope of a linear regression of the approximately straight force-indentation curve (up to 10 μm) yielded the stiffness of the brain at the

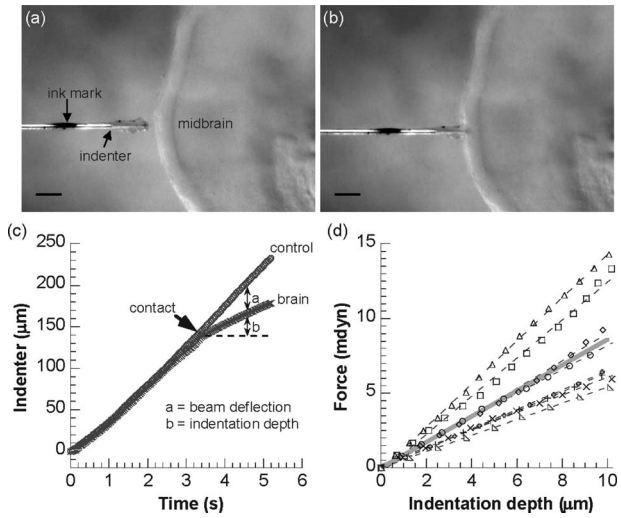

Fig. 3 Microindentation tests on a chick brain. (*a*)–(*b*) Video micrographs showing the indenter tip (with an ink mark) approaching (*a*) and indenting (*b*) the midbrain region of a stage-12 chick brain. The brain is held by a micropipette on the opposite side of the indenter (scale bar is 100 μm). (*c*) Beam deflection and indentation depth are determined from the indenter tip displacements between control (no contact) and actual indentations. The product of beam deflection with beam stiffness yields indentation force. (*d*) All experimental force-indentation curves (symbols, $n=8$) for the stage-12 midbrain. The slopes of linear regressions (dashed lines) to these curves yield stiffness values for each tested midbrain, the average of which is represented by the solid gray line.

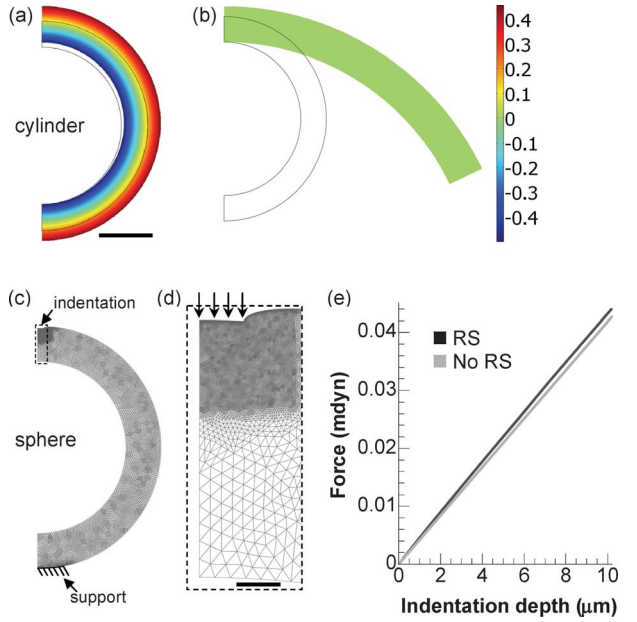

Fig. 4 Finite-element modeling of the effect of residual stress on indentation stiffness. (*a*) Distribution of circumferential residual stress ($\sigma_\theta^* = \sigma_\theta/\mu$) in unloaded cylinder model after specified growth. The geometry after growth is close to the average stage-12 midbrain (scale bar is 100 μm for (*a*)–(*c*)). (*b*) Approximate zero-stress state of the cylinder after a simulated cut. The opening angle (116 deg) is close to the average experimental value (108 deg) for the stage-12 midbrain (see Fig. 7(*a*)). (*c*) Model of indenting a residual stress-containing sphere (rendered in wire frames). The geometry and residual stress distributions are approximately the same as those of the cylinder model in (*a*). (*d*) Close-up of the region near the indenter tip (dashed rectangle in (*c*)). Arrows indicate the specified boundary displacement to simulate indentation (scale bar is 10 μm). (*e*) Force-indentation curves for sphere models of the same geometry with and without residual stress (RS). Residual stress has a relatively small effect on indentation stiffness.

indented region (Fig. 3(*d*)). At each stage, the stiffness in each region was obtained from 5–11 chick embryos. One-way ANOVA tests were used to compare the regional indentation stiffness at each stage.

2.3 Finite-Element Models. Regional stiffness depends on both material properties and geometry. In addition to microindentation tests, finite-element models are needed to estimate the material properties of the brain. Three types of models were created.

(1) 2D cylindrical and spherical models were used to explore the effect of residual stress on stiffness measurements. (These effects were found to be relatively small).
(2) 3D indentation models for the brain tube at each stage (without residual stress) were used to determine material properties.
(3) Models of simplified brain geometry were used to help interpret the experimental results.

It is important to note that, although the indentation depth in the experiments is relatively small compared with the wall thickness, large strains can occur close to the indenter. Hence, all models in this paper include the nonlinearities associated with large deformations.

2.3.1 Models for the Effect of Residual Stress. To get a sense for the significance of residual stress in our stiffness measurements, we studied two limiting cases that can be simulated in two dimensions (2D)—a cylinder in plane-strain and a sphere undergoing axisymmetric deformation. For these preliminary parametric studies, 2D models are highly desirable because they are significantly more efficient to build and run than comparable 3D models. The sphere is the simplest geometry that can capture the effects of residual stress on indentation in a 2D finite-element model. The cylinder model was used to obtain the residual stress distribution in a brain slice that would produce an opening angle close to the experimental mean for the stage-12 midbrain. A similar residual stress distribution was then introduced in the sphere model, which was indented.

First, we created a nonlinear plane-strain (cylinder) model for a section of a stage-11 chick midbrain using the commercial finite-element software COMSOL Multiphysics (V.3.3, COMSOL AB, Burlington, MA). Residual stress was introduced by specifying volumetric growth across the wall to achieve geometry and opening angles similar to those measured for the stage-12 midbrain (Fig. 4(*a*) and 4(*b*)). Due to symmetry, only half of the brain was analyzed with appropriate symmetry conditions specified. Growth was simulated using the theory presented by Rodriguez et al. [13], which can be readily implemented in COMSOL (see details in Ref. [14]). Briefly, starting with the zero-stress configuration (the smaller outline in Fig. 4(*a*)), each material element grows according to a specified growth deformation gradient tensor $\mathbf{F}_g$. The geometric compatibility among elements requires elastic deformation $\mathbf{F}_e$ that in turn causes residual stresses in the unloaded brain. Thus, the total deformation is described by $\mathbf{F}=\mathbf{F}_e\cdot\mathbf{F}_g$ ($\mathbf{F}_g=\mathbf{I}$ for no net growth with $\mathbf{I}$ being the identity tensor). The major deformation variable is $\mathbf{F}$, $\mathbf{F}_g$ is specified, and the stresses depend on $\mathbf{F}_e=\mathbf{F}\cdot\mathbf{F}_g^{-1}$. Here, axisymmetric growth was specified in the radial and circumferential directions, i.e., $\mathbf{F}_g=\lambda_{gr}\mathbf{e}_r\mathbf{e}_r+\lambda_{g\theta}\mathbf{e}_\theta\mathbf{e}_\theta$, where the λ_{gi} are growth stretch ratios relative to the undeformed cylindrical polar coordinates (r, θ) and $\mathbf{e}_i$ are the corresponding local unit vectors [15]. For representative material properties (see below), the following differential growth was found to produce proper brain geometry (radius and wall thickness) and opening

angle (one of the two vertical boundaries was set free) in the cylinder model: $\lambda_{gr}=1.4$ and $\lambda_{g\theta}=1+0.5\cdot(r_o/r-1)$, where r_o is the undeformed outer radius of the brain section (Figs. 4(*a*) and 4(*b*)).

To a first approximation, the neuroepithelium is assumed to be an isotropic, nearly incompressible, pseudoelastic material characterized by the modified neo-Hookean strain-energy density function

$$W=\frac{1}{2}\mu(I_1J_e^{-2/3}-3)+p\left(1-J_e-\frac{p}{2\kappa}\right)$$

where μ and κ are the small-strain shear and bulk modulus, respectively, I_1 is the first invariant of the right Cauchy–Green deformation tensor (given by $\mathbf{F}_e^T\cdot\mathbf{F}_e$), $J_e=\det\mathbf{F}_e$ is the elastic volume ratio, and p is a penalty variable introduced for nearly incompressible materials. The Cauchy stress tensor is given by the constitutive relation $\boldsymbol{\sigma}=J_e^{-1}\,\mathbf{F}_e\cdot\partial W/\partial\mathbf{F}_e^T$ and stresses are normalized relative to the shear modulus (e.g., circumferential stress $\sigma_\theta^*=\sigma_\theta/\mu$ in Fig. 4). For numerical stability, we took the bulk modulus (κ) to be three orders of magnitude larger than μ.

Local indentation cannot be simulated in a plane-strain model for a cylinder because deformation would be imposed along the entire length of the cylinder. Hence, using the results from the cylindrical model, we next developed a spherical indentation model as a simple representation for a brain vesicle. Axisymmetric deformation is assumed, i.e., all variables depend only on the radial and meridional coordinates r and θ, respectively (φ is the circumferential coordinate). With the initial cross-sectional geometry taken to be the same as that of the cylinder model, the following growth was found to produce geometry and residual stress distributions in the sphere model similar to those in the cylinder model: $\lambda_{gr}=1.24$ and $\lambda_{g\theta}=\lambda_{g\varphi}=1+0.3\cdot(r_o/r-1)$. Following growth, a small circular boundary (10 μm radius) on top of the sphere was specified to move downwards, mimicking the indentation, while an area (100 μm in diameter) on the opposite side was fixed to simulate the pipette support (Fig. 4(*c*)). Stiffness is defined as the slope of the linear regression fit to the force-displacement curve (Fig. 4(*e*); regressions not shown).

In addition, the geometry after growth (close to the average size of the stage-12 midbrain) was used to establish another spherical indentation model that contained no residual stress (not shown). The indentation results from these two models were compared to examine how residual stress affects the indentation stiffness.

2.3.2 Models for Estimating Material Properties. To estimate the material properties from the microindentation experiments, nonlinear 3D finite-element models for the stage 11–13 chicken brain were created, using the finite-element software ABAQUS (v.6.7, Abaqus, Inc., Providence, RI). For simplicity, because the above 2D models show that residual stress has little effect on the measured stiffness (see Sec. 3), residual stresses are not included in these models. The models resemble the overall morphology of the chick brain at each stage but the optic vesicles in the forebrain are not included (Fig. 5(*a*)–5(*c*)). Due to symmetry, only one longitudinal half of the brain needs to be analyzed with symmetry conditions specified accordingly. The indenter tip is simulated as a rigid cylinder with frictionless contact specified between the surfaces on the indenter tip and the brain tube. A small circular area (100 μm diameter) of the brain tube on the opposite side of the indenter tip is fixed to simulate the pipette support (Fig. 5(*a*)). Other boundaries are free. The geometry is partitioned into 10^6 (order of magnitude) linear tetrahedral elements (Fig. 5), with the mesh being further refined near the indentation region (see close-up in Fig. 5(*e*)). The sufficiency of the mesh density was confirmed by solving the problem for increasing mesh densities. Similar procedures were adopted for all regions to be tested.

As a first approximation, we assume that all regions of the brain possess the same material properties. Again, the wall is assumed to be composed of an isotropic, nearly incompressible neo-Hookean material characterized by the shear modulus (μ) and bulk modulus (κ, three orders of magnitude larger than μ), respectively. The indentation stiffness was obtained by linearly fitting the initial force-indentation curve (up to 20 μm indentation).

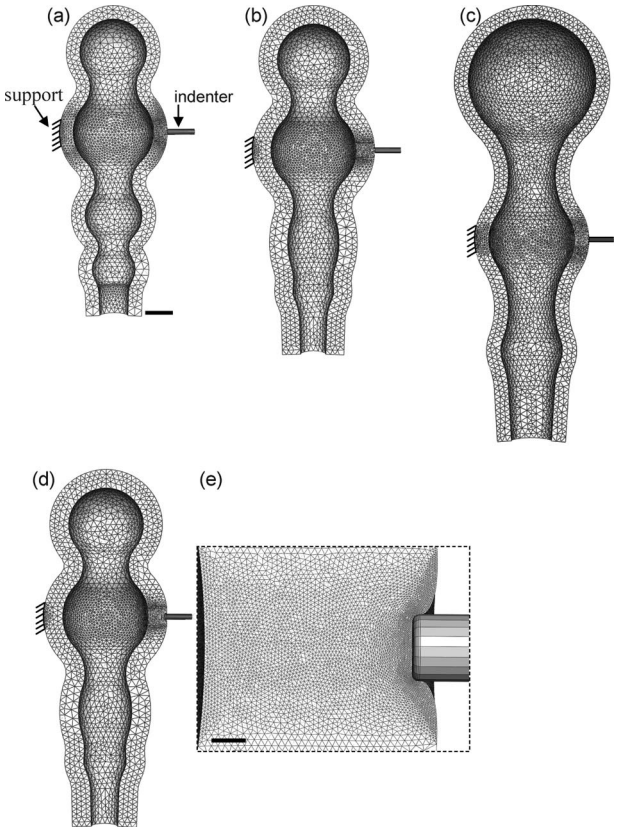

Fig. 5 Finite-element models for estimating material properties. (*a*)–(*c*) 3D models for indenting the midbrain region at stages 11, 12, and 13, respectively. Undeformed model geometries resemble the overall morphology of the chick brain at each stage. The forebrain region is simplified without optic vesicles. Scale bar in (*a*) represents 100 μm for (*a*)–(*d*). (*d*) Deformed model geometry showing the stage-12 midbrain being indented about 20 μm. (*e*) Close-up near the indenter tip in (*d*) (scale bar is 10 μm).

At each stage, a value of the shear modulus was obtained for each region by matching the stiffness from the indentation model to the average stiffness for the same region from the experiments. These data were used to compute a mean shear modulus for each stage. For statistical comparison of shear moduli from different stages, one-way ANOVA test was used.

2.3.3 Models for Interpreting Experimental Results. For better understanding of how local geometry (e.g., hills versus valleys) of the brain tube affects the indentation results, we created several 3D models in ABAQUS that possess the same cross-sectional geometry (as the average stage-12 midbrain region) at the indentation site but different overall longitudinal curvatures (Fig. 6). These geometrical variations include longitudinally convex (part of a sphere), straight (cylinder), and concave curvatures relative to the indenter position (Fig. 6(*a*)–6(*c*), respectively). For comparison, an additional model of a smaller straight cylinder (not shown) was also created that possesses the same cross-sectional geometry as the average stage-12 MH valley (the same wall thickness but only half the inner diameter of the midbrain section). Due to symmetry, only a quarter of the geometry was analyzed with symmetry conditions specified, accordingly. All other procedures for material, mesh, and indentation contact are similar to those discussed above for the 3D brain models.

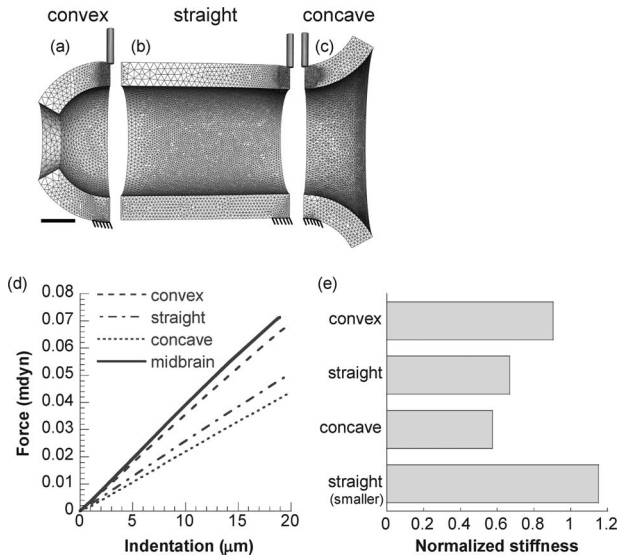

Fig. 6 Finite-element models for studying effects of local geometry on indentation. (*a*)–(*c*) Models showing 20 μm indentation on a longitudinally convex, straight, and concave cylinder, respectively. Scale bar in (*a*) represents 100 μm for (*a*)–(*c*). (*d*) Force-indentation curves from these models. Solid line is from the model for the stage-12 midbrain shown in Fig. 5(*d*). (*e*) Stiffnesses given by the models where the stiffness values are the slopes of force-indentation curves from linear regressions and are normalized by that from the model for the stage-12 midbrain. See text for details.

3 Results

3.1 Opening Angles. When a radial cut was made, the brain slice sprang open immediately (Fig. 2(*c*)). Overall, the average opening angles of the stage 11–13 chick brain sections ($n=7-10$ for most regions at each stage) varied from 40 deg to 110 deg (Fig. 7(*a*)). At stage 11, opening angles were significantly different between midbrain hill (*M*) and MH valley ($p<0.005$) and between FM and MH valleys ($p<0.05$). At stage 12, the only significant difference in opening angles was between midbrain hill and MH valley ($p<0.005$). At stage 13, there was no significant difference in opening angles between regions ($p>0.1$). From stage 11–13, only the opening angles at the FM valley region changed significantly ($p<0.05$).

Despite mixed statistical results at each developmental stage, the average opening angles in the hill regions tended to be larger than those in the narrower valley regions (Fig. 7(*a*)). For each region (except the FM valley) during development, the average opening angle seemed to increase first from stage 11 to stage 12 and then decrease to a smaller magnitude at stage 13.

3.2 Indentation Stiffness and Wall Shear Modulus. The peak indentation depth in the experiments was about 10 μm or about 15% of the wall thickness. The stiffness of the early chick brain from the microindentation tests ranged from $\sim$0.4 mdyn/μm to 1 mdyn/μm ($n=5-10$ for each region at each stage, Fig. 7(*b*)). At each developmental stage (11–13), variations in the indentation stiffness among different regions were not statistically significant, although there appears to be a general trend of increasing average stiffness for most regions as the brain develops (Fig. 7(*b*)).

Because the shape and size of the brain changes dramatically from stage 11 to stage 13 (Fig. 1), indentation stiffness alone cannot be used as an indicator for changes in material properties during development. Hence given the geometry, the 3D indentation model (Fig. 5) was used to estimate the shear modulus (μ) of the brain at each stage. As described in Sec. 2, the value of μ for

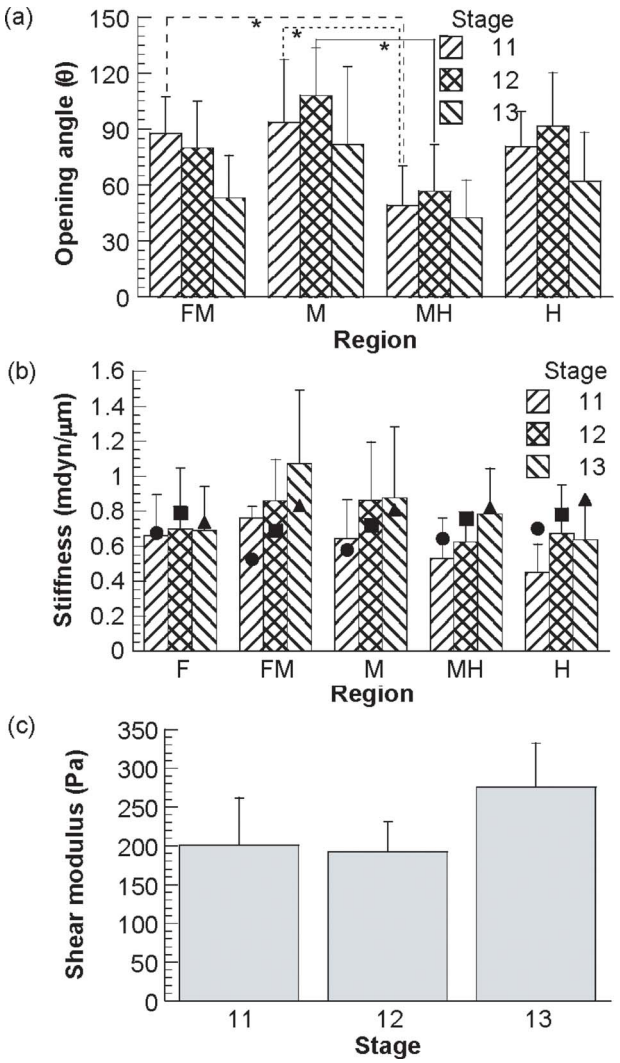

Fig. 7 Opening angles and material properties of chick brains at stages 11–13. (*a*) Regional opening angles where asterisks (*) represent statistically significant difference between two regions at each stage, (*b*) regional indentation stiffness from experiments (columns with error bars) and models (filled symbols), and (*c*) shear moduli computed from models in Fig. 5. Error bars represent standard deviations.

each region was determined by matching the stiffness from the indentation model to the average measured stiffness for the same region. These data then provided an average modulus for each stage. The average values of μ for stages 11–13 chick brains were about 201 Pa, 192 Pa, and 276 Pa, respectively, (Fig. 7(*c*)). There was no significant change in wall shear modulus from stage 11 to stage 13 ($p>0.5$). The overall average value of the shear modulus during the studied stages is about 220 Pa.

Next, we used the brain models for each stage (Figs. 5(*a*)–5(*c*)), along with the average modulus for the same stage (Fig. 7(*c*)), to compute an indentation stiffness for each region. In general, the trends in the measured and computed stiffnesses agree reasonably well (Fig. 7(*b*)). These results suggest that the modulus is approximately independent of age and position during the studied stages.

3.3 Residual Stress Has Negligible Effect on Indentation Stiffness. Residual stress can greatly affect mechanical properties of soft tissue as determined from microindentation tests [16]. The significance of these effects depends on the magnitude of the stress and the structure of the tissue. We used computational models to examine how residual stress affects embryonic brain me-

chanics. First, differential volumetric growth was specified in an unloaded cylinder to create residual stress with circumferential compression near the inner layers and tension near the outer surface (Fig. 4(*a*)). Simulating a radial cut released the residual stress (Fig. 4(*b*)), yielding a zero-stress arc characterized by an opening angle (116 deg) close to the average experimental value (108 deg for the stage-12 midbrain region). Next, growth was specified in a spherical model for a brain vesicle (Figs. 4(*c*) and 4(*d*)), yielding residual stresses similar to those in the cylinder model. The indentation stiffness for the sphere with residual stress was only about 3% higher than that given by indenting a stress free sphere of the same material and geometry (not shown, Fig. 4(*e*)). These results indicate that residual stress has a relatively small effect on the stiffness probed by the microindentation tests. For simplicity, therefore, residual stress was not included in our 3D models.

3.4 Characteristic Brain Geometry Gives Nearly Uniform Stiffness. As expected, the stiffness of a cylinder with a given wall thickness increases as the radius decreases (see Fig. 6(*e*) for straight tube). Surprisingly however, but consistent with our experimental measurements, the 3D model predicts that hills and valleys have roughly the same indentation stiffness (Fig. 7(*b*)) despite having considerably different radii (for the same modulus and wall thickness). To investigate this phenomenon, we created several different models that possess different longitudinal curvature (Figs. 6(*a*)–6(*c*)). Unless noted otherwise, the radius and the wall thickness at the indentation site are the same for all models as those for a stage-12 midbrain section. To simplify comparison, all the stiffness values are normalized by the indentation stiffness of the stage-12 midbrain, as provided by the realistic 3D model shown in Fig. 5(*d*). The results indicate that the stiffness of the convex cylinder (0.90) is higher than that of the straight (0.67) and concave cylinders (0.57) (Figs. 6(*d*) and 6(*e*)).

For the brain tube, these results suggest that, in a valley, stiffening due to a smaller radius (relative to a hill) is effectively cancelled by the softening effect of the concave curvature. These combined effects produce a brain tube of nearly uniform indentation stiffness (Fig. 7(*b*)).

4 Discussion

During early development, the embryonic chick brain undergoes rapid growth and expansion in response to increasing luminal pressure, and the major subdivisions along the brain tube become more and more prominent (Fig. 1). To understand the mechanisms that drive morphogenesis of the brain tube, the mechanical response to the increasing cavity pressure must be determined. This requires knowledge of the mechanical properties of embryonic brain tissue, which have not been previously explored.

In this study, we found that considerable residual stress exists in the early chick brain, which can be characterized by the opening angle (Fig. 2). Although the variations are not statistically significant, the average opening angles at each stage seem to exhibit a pattern, i.e., larger opening angles in the hill regions and smaller ones in the valley regions (Fig. 7(*a*)). This spatial pattern might indicate differential growth between hill and valley regions. Moreover, our data indicate that the temporal change in the average opening angle for each region (except the FM valley) is similar to the change in the opening angle of blood vessels during pressure increase [17], whereby the angle first increases and then decreases. From these results, we speculate that the inner side of the neuroepithelium first grows in response to higher circumferential stress near the lumen from stage 11 to stage 12, giving higher residual compression near the inner radius and thus larger opening angles. By stage 13, the outer layers grow relatively faster, causing opening angles to decrease. However, unlike multilayered blood vessels, the early brain is composed of only a single neuroepithelial cell layer. Therefore, the adaptation mechanisms of the early brain to increasing pressure may be different. This behavior warrants further study.

Surprisingly, at each stage the measured stiffness was approximately the same at all locations, despite considerable differences in geometry (Fig. 7(*b*)). Investigating this behavior with idealized models, we found that indentation stiffness is higher for convex curvature and smaller radius but lower for concave curvature and larger radius (Fig. 6(*e*)). Hence, geometric effects in the hills (convex curvature and larger radius) and the valleys (concave curvature and smaller radius) essentially cancel out, giving nearly uniform indentation stiffness. Our measurements and calculations also suggest that the shear modulus is approximately uniform and independent of developmental stage (Figs. 7(*b*) and 7(*c*)).

It is important to note that these results were obtained for relatively small indentations; future work should determine nonlinear material properties of the brain from large-indentation tests. Nevertheless, it is interesting to consider the possibility that these characteristics result from some optimization principle in brain development. Even before the brain tube seals and cerebrospinal fluid pressure begins to rise, the brain tube contains relatively small but distinct vesicles (hills) separated by constrictions (valleys). Genetic and chemical activity may produce this initial pattern. Then, as the lumen pressure increases, Laplace's law gives the average circumferential stress $\sigma_\theta = pr/h$, where p is the pressure, r is the radius, and h is the wall thickness. Hence, for uniform h, the different radii dictate that the average stress in the hills is larger than in the valleys. If growth rate increases with stress [10], then the hills would grow faster than the valleys, leading to further relative expansion of the vesicles driven by positive feedback. Therefore, the geometric and mechanical characteristics of the brain tube may be optimized to facilitate brain vesicle expansion and differentiation in response to increasing cavity pressure.

A previous study has determined the nonlinear material properties of the stage-12 chick heart during cardiac looping [18]. The average shear moduli of the chick myocardium and cardiac jelly at stage 12 are approximately 26 Pa and 6 Pa [18], respectively. Thus, the shear modulus of the early chick brain is an order of magnitude greater than that of the heart. On the other hand, shear moduli for the embryonic chick brain are surprisingly similar to those (100–1000 Pa) measured for animals in various species and ages [19–22], despite dramatic differences in components and structure between embryonic and fully developed brains [9]. The primary steps of brain development include generation and differentiation of neurons from neural stem cells and their subsequent migration and maturation [9]. Mature brains are composed of gray matter containing neuronal cell bodies and white matter containing interconnected axonal fibers. In general, mechanics of the mature brain is important in modeling and understanding of traumatic brain injury and neurosurgery [23]. For example, during neurosurgical procedures, the human brain behaves like a compressible viscoelastic solid [23]. All of these results, however, might be affected by various conditions during testing [24].

Residual stress was not included in our 3D models. A previous study showed that residual stress can greatly affect the stiffness and material properties determined from microindentation tests of soft tissue [16]. For the brain tube, however, our models show that normal levels of residual stress have little effect on overall indentation stiffness.

The spatial distribution of residual stresses in the early brain, as manifested by opening angles, might provide an optimal mechanical environment for dividing neural stem cells. From a mechanics point of view, residual stresses can help make stress distributions relatively uniform across the wall of a pressurized tube, e.g., blood vessels [25]. The wall of the early brain tube is composed of a single layer of pseudostratified neural stem cells or neuroepithelium [9]. The nuclei of these cells migrate radially within the cell body during the cell cycle [9]. The opening angle results show that circumferential residual stresses exist throughout the brain tube at all stages (Fig. 7(*a*)). With these residual stresses, the unloaded (stage 11) or initially pressurized brain (stage 12) would be under tensile stresses in the outer layers and compressive

stresses in the inner layers of the wall (Fig. 4(*a*)). Therefore, the nuclei are under tension when they are located near the outside of the brain tube where DNA synthesis occurs. The nuclei move toward the lumen as the cell cycle proceeds and would be under compression near the luminal side of the brain when mitosis occurs. However, as tensile forces are usually generated during mitosis to separate the chromosomes [26], it is likely that overall compression in the inner layers of the early brain could hinder, if not control, the neural dividing process. During morphogenesis, compressive stresses generally reduce, whereas tensile stresses increase, proliferation rates (see review in Ref. [10]). As luminal pressure increases later during development [6,7], the inner layers of the brain tube would also be under tension, which could facilitate faster division of neural stem cells.

The above speculation is consistent with the following findings: (1) early brain enlargement requires luminal pressure [1]; (2) the brain cavity expands faster than the tissue grows at the beginning (stage 11–12) of brain enlargement (proliferation slowed by compression), but soon (after stage 13) the reverse is true (proliferation facilitated by tension) [3]; and (3) sustained hyperpressure promotes higher mitotic activity [6].

Much work is needed to learn the role of mechanics in regulating proliferation of neural stem cells. Information provided in this study on the residual stress and material properties of the early brain will help illuminate the mechanical environment of such cells and the process of early brain morphogenesis.

Acknowledgment

We thank Krikor Dikranian for helpful discussions and suggestions. This work was supported by the National Institutes of Health (Grant No. R01 GM075200) and the National Science Foundation (Grant No. DMS-0540701).

References

[1] Desmond, M. E., and Jacobson, A. G., 1977, "Embryonic Brain Enlargement Requires Cerebrospinal Fluid Pressure," Dev. Biol., **57**, pp. 188–198.
[2] Desmond, M. E., and O'Rahilly, R., 1981, "The Growth of the Human Brain During the Embryonic Period Proper," Anat. Embryol. (Berl), **162**, pp. 137–151.
[3] Pacheco, M. A., Marks, R. W., Schoenwolf, G. C., and Desmond, M. E., 1986, "Quantification of the Initial Phases of Rapid Brain Enlargement in the Chick Embryo," Am. J. Anat., **175**, pp. 403–411.
[4] Schoenwolf, G. C., and Desmond, M. E., 1984, "Neural Tube Occlusion Precedes Rapid Brain Enlargement," J. Exp. Zool., **230**, pp. 405–407.
[5] Hamburger, V., and Hamilton, H. L., 1951, "A Series of Normal Stages in the Development of the Chick Embryo," J. Morphol., **88**, pp. 49–92.
[6] Desmond, M. E., Levitan, M. L., and Haas, A. R., 2005, "Internal Luminal Pressure During Early Chick Embryonic Brain Growth: Descriptive and Empirical Observations," Anat. Rec., **285A**, pp. 737–747.
[7] Jelínek, R., and Pexiedner, T., 1968, "The Pressure of Encephalic Fluid in Chick Embryos Between the 2nd and 6th Day of Incubation," Physiol. Bohemoslov., **17**, pp. 297–305.
[8] Desmond, M. E., and Levitan, M. L., 2002, "Brain Expansion in the Chick Embryo Initiated by Experimentally Produced Occlusion of the Spinal Neurocoel," Anat. Rec., **268**, pp. 147–159.
[9] Gilbert, S. F., 2006, *Developmental Biology*, 8th ed., Sinauer Associates, Inc., Sunderland, MA.
[10] Wozniak, M. A., and Chen, C. S., 2009, "Mechanotransduction in Development: A Growing Role for Contractility," Nat. Rev. Mol. Cell Biol., **10**, pp. 34–43.
[11] Voronov, D. A., and Taber, L. A., 2002, "Cardiac Looping in Experimental Conditions: Effects of Extraembryonic Forces," Dev. Dyn., **224**, pp. 413–421.
[12] Zamir, E. A., Srinivasan, V., Perucchio, R., and Taber, L. A., 2003, "Mechanical Asymmetry in the Embryonic Chick Heart During Looping," Ann. Biomed. Eng., **31**, pp. 1327–1336.
[13] Rodriguez, E. K., Hoger, A., and McCulloch, A. D., 1994, "Stress-Dependent Finite Growth in Soft Elastic Tissues," J. Biomech., **27**, pp. 455–467.
[14] Taber, L., 2008, "Theoretical Study of Beloussov's Hyper-Restoration Hypothesis for Mechanical Regulation of Morphogenesis," Biomech. Model. Mechanobiol., **7**, pp. 427–441.
[15] Taber, L. A., and Perucchio, R., 2000, "Modeling Heart Development," J. Elast., **61**, pp. 165–197.
[16] Zamir, E. A., and Taber, L. A., 2004, "On the Effects of Residual Stress in Microindentation Tests of Soft Tissue Structures," ASME J. Biomech. Eng., **126**, pp. 276–283.
[17] Fung, Y. C., and Liu, S. Q., 1989, "Change of Residual Strains in Arteries Due to Hypertrophy Caused by Aortic Constriction," Circ. Res., **65**, pp. 1340–1349.
[18] Zamir, E. A., and Taber, L. A., 2004, "Material Properties and Residual Stress in the Stage 12 Chick Heart during Cardiac Looping," ASME J. Biomech. Eng., **126**, pp. 823–830.
[19] Gefen, A., Gefen, N., Zhu, Q. L., Raghupathi, R., and Margulies, S. S., 2003, "Age-Dependent Changes in Material Properties of the Brain and Braincase of the Rat," J. Neurotrauma, **20**, pp. 1163–1177.
[20] Georges, P. C., Miller, W. J., Meaney, D. F., Sawyer, E. S., and Janmey, P. A., 2006, "Matrices With Compliance Comparable to That of Brain Tissue Select Neuronal Over Glial Growth in Mixed Cortical Cultures," Biophys. J., **90**, pp. 3012–3018.
[21] Prange, M. T., and Margulies, S. S., 2002, "Regional, Directional, and Age-Dependent Properties of the Brain Undergoing Large Deformation," ASME J. Biomech. Eng., **124**, pp. 244–252.
[22] Thibault, K. L., and Margulies, S. S., 1998, "Age-Dependent Material Properties of the Porcine Cerebrum: Effect on Pediatric Inertial Head Injury Criteria," J. Biomech., **31**, pp. 1119–1126.
[23] Kyriacou, S. K., Mohamed, A., Miller, K., and Neff, S., 2002, "Brain Mechanics for Neurosurgery: Modeling Issues," Biomech. Model. Mechanobiol., **1**, pp. 151–164.
[24] Hrapko, M., van Dommelen, J. A. W., Peters, G. W. M., and Wismans, J. S. H., 2008, "The Influence of Test Conditions on Characterization of the Mechanical Properties of Brain Tissue," ASME J. Biomech. Eng., **130**, p. 031003.
[25] Fung, Y. C., 1998, *Biomechanics: Motion, Flow, Stress, and Growth*, 2nd ed., Springer, New York.
[26] Sharp, D. J., Rogers, G. C., and Scholey, J. M., 2000, "Microtubule Motors in Mitosis," Nature (London), **407**, pp. 41–47.